EurJIC
European Journal of Inorganic Chemistry

A Journal of
ChemPubSoc Europe

Accepted Article

Title: Cyanide bridged FeII-MI bimetallic Hofmann-like spin-crossover coordination polymers based on 2,6-Naphthyridine

Authors: Lucía Piñeiro-López, Francisco Javier Valverde-Muñoz, Maksym Seredyuk, Carlos Bartual-Murgui, M. Carmen Munoz, and Jose Antonio Real

To be cited as: *Eur. J. Inorg. Chem.* 10.1002/ejic.201700920

Link to VoR: http://dx.doi.org/10.1002/ejic.201700920

WILEY-VCH

Cyanide bridged Fe^{II}-M^{I} bimetallic Hofmann-like spin-crossover coordination polymers based on 2,6-Naphthyridine

Lucía Piñeiro-López,[a] Francisco-Javier Valverde Muñoz,[a] Maksym Seredyuk,[a] Carlos Bartual Murgui,[a] M. Carmen Muñoz,[b] José Antonio Real*[a]

Abstract: Two new 3D spin crossover (SCO) Hofmann-type coordination polymers {Fe(*2,6-naphthy*)[Ag(CN)$_2$][Ag$_2$(CN)$_3$]} (**1**) and {Fe(*2,6-naphthy*)[Au(CN)$_2$]$_2$}·(0,5)PhNO$_2$ (**2**) (*2,6-naphthy* = 2,6-naphthyridine) have been synthesized and characterized. Both derivatives are made up of infinite stacks of {Fe[Ag(CN)$_2$]$_2$[Ag$_2$(CN)$_3$]}$_n$ and {Fe[Au(CN)$_2$]$_2$}$_n$ layered grids pillared by 2,6-Naphthy ligands coordinated to the axial positions of the Fe^{II} centers of alternate layers. The *in situ* generated [Ag$_2$(CN)$_3$]$^-$ linkers define wide rectangular windows that favor the interpenetration of three identical 3D networks, strong argentophilic interactions between them and generation of a densely packed structure without accessible void spaces. In contrast, the smaller rhombus-shaped windows' size in **2** affords a structure made up of doubly interpenetrated 3D networks with strong aurophilic interactions between them and accessible voids partially occupied by nitrobenzene molecules. **1** displays a relatively abrupt two-step SCO in the temperature interval 150-215 K whereas **2** features an incomplete one-step SCO behavior ($T_{1/2}$ = 166 K) that extends over 150 K.

Introduction

Iron(II) spin crossover (SCO) complexes are a well-known class of switchable molecular materials. The switching between the high-spin (HS) and low-spin (LS) states occurs in a reversible, controllable and detectable manner triggered by external stimuli (i.e. temperature, pressure, light, or guest molecules) involving changes in the molecular structure, magnetism, color and electrical polarizability.[1] The different size of the Fe^{II} ion in both electronic states, is at the origin of cooperative elastic interactions between the SCO centers in the crystal.[2] When these interactions are strong enough, the SCO material exhibits bistability, an appealing property with potential application in the construction of molecular devices for information storage, signal processing and sensing.[3] In this respect, amenability to process the SCO materials at micro- and nano-metric scales or even at single molecule level has aroused in the last years much interest in the areas of molecular nanoelectronics and spintronics.[4]

The design and synthesis of new SCO materials is a necessary step to discover interesting SCO behaviors and possible applications. The impressive cooperative properties displayed by the first one- (1D) and two-dimensional (2D) 1,2,4-triazole-based Fe^{II} SCO coordination polymers suggested that cooperativity could be enhanced by replacing the intermolecular interactions between SCO centers with more reliable coordination bonds afforded by suitable bridging ligands.[5,3d] Consequently, the polymeric approach systematically explored from the 1990s has afforded a number of relevant two-(2D) and three-dimensional (3D) SCO coordination polymers (SCO-CP) and porous metal-organic frameworks (SCO-MOFs).[6]

One of the most prolific series of SCO-CPs/SCO-MOFs are constituted by cyanide-bridged Fe-$M^{I,II}$ bimetallic 2D and 3D Hofmann-like compounds. In particular the use of dicyanometallate linkers such as [M^{I}(CN)$_2$]$^-$ (M^{I} = Ag^{I} and Au^{I}) has been fostered since the first 3D complexes {Fe(*L*)$_x$[Ag^{I}(CN)$_2$]$_2$} reported in 2002.[7] In particular, the complex {Fe(*pz*)[Ag^{I}(CN)$_2$]$_2$} (*pz* = pyrazine) is prototypal of a series of SCO complexes generically formulated {Fe(*L*)[M^{I}(CN)$_2$]$_2$} (M^{I} = Ag and Au) where *L* is a bis-monodentate bridging pyridine-like ligand. The linear [M^{I}(CN)$_2$]$^-$ anions occupy the equatorial coordination positions of the Fe^{II} ions defining an infinite stack of 2D [Fe{M^{I}(CN)$_2$}$_2$]$_\infty$ layers pillared by the bridging ligand *L* which occupy axial positions of the Fe^{II} ions. The layers are organized in such a way that the ligands *L* thread the meshes of adjacent sheets generating two identical interpenetrated 3D networks with the α-Po topology (Scheme I). While {Fe(*pz*)[Ag^{I}(CN)$_2$]$_2$} is LS at temperatures below 400 K, it has been recently demonstrated that the homologous Au^{I} derivative displays a cooperative SCO between 367 and 349 K.[8] Even more cooperative SCO between 261 and 223 K has been observed for the corresponding 2-fluoropyrazine (*Fpz*) and M^{I} = Au derivative.[9] Notably, when using longer bridging ligands such as *bipytz*,[10] *bpmp*,[11] *bpp*,[12] or *dpb*[13] (Scheme 1), and M^{I} = Au, interesting inclusion chemistry and cooperative SCO behaviors have been described despite interpenetration. In summary, the use of different organic ligands and cyanometallate anions has resulted in a Hofmann-type family, which exhibit customized SCO behaviors coupled with other interesting properties.[6]

Continuing this work, herein we report the synthesis, crystal structures and physical properties of two novel Fe^{II} SCO systems based on the bis-monodentate organic ligand 2,6-naphthyridine (*2,6-naphthy*) formulated {Fe(*2,6-naphthy*)[Ag(CN)$_2$][Ag$_2$(CN)$_3$]} (**1**) and {Fe(*2,6-naphthy*)[Au(CN)$_2$]$_2$}·(0.5)PhNO$_2$ (**2**) (PhNO$_2$ = nitrobenzene as guest molecule).

[a] L. Piñeiro-López, F. J. Valverde-Muñoz, M. Seredyuk, C. Bartual-Murgui, J. A. Real
Institut de Ciència Molecular (ICMol), Departament de Química Inorgànica
Universitat de València
C/ Catedrático José Beltrán Martínez, 2, 46980 Paterna (Valencia), Spain
E-mail: jose.a.real@uv.es; www.uv.es/smolmat
[b] M. C. Muñoz
Departament de Física Aplicada
Universitat Politècnica de València
Camino de Vera s/n, 46022 Valencia, Spain

Supporting information for this article is given via a link at the end of the document.

Scheme 1. Schematic view of two interpenetrated 3D networks with the α-Po topology and representation of the mentioned ligands.

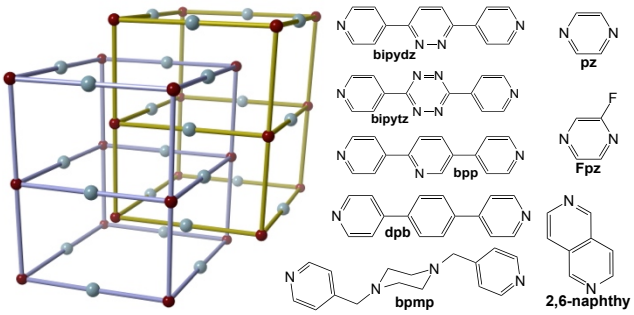

Results

Synthesis. The *2,6-naphthy* ligand was synthetized following a modified synthetic route (Supporting Information, Section 1.8.1). Single crystals of **1** and **2** were synthesized by means of slow liquid-liquid diffusion techniques using a modified (common) H-vessel tube. Red and yellow rod-like single crystals of **1** and **2**, respectively, were formed with relative high yield (ca. 50%) four weeks later. In particular, the occurrence of the relatively rare $[Ag_2(CN)_3]^-$ species in **1**, which have been previously identified in crystals of some related SCO-CPs[14] but, as far as we know, it has never been observed in solution or isolated in crystals as discrete anions of single salts. The incorporation of either $[Ag(CN)_2]^-$ or a mix of $[Ag(CN)_2]^-$ and $[Ag_2(CN)_3]^-$ into the final polymer is most likely the result of competition between the two moieties and their associated equilibria (eq. [i] and [ii]). This competition seems to be influenced by the solvent medium, reagent concentrations and overall stability and solubility of the final product. In **1**, low concentration of $[Ag^I(CN)_2]^-$ and extended reaction time (liquid-liquid diffusion method) seems to favor the dissociation of $[Ag^I(CN)_2]^-$ to give $[Ag^I{}_2(CN)_3]^-$. However, in the chosen experimental conditions the synthesis of **1** is perfectly reproducible.

$$[Ag^I(CN)_2]^- \leftrightarrow CN^- + Ag^ICN \qquad [i]$$

$$Ag^ICN + [Ag^I(CN)_2]^- \leftrightarrow [Ag^I{}_2(CN)_3]^- \qquad [ii]$$

The presence and quantification of nitrobenzene molecules in **2** were confirmed by single-crystal X-ray diffraction studies and thermogravimetric analysis (Figure S1, Supporting Information).

Magnetic properties. The plot of $\chi_M T$ vs. T for **1**, where $\chi_M T$ is the molar magnetic susceptibility and T is the temperature, is displayed in Figure 1-top. At 250 K, the $\chi_M T$ value ca. 3.75 cm^3 K mol^{-1} is consistent with all Fe^{II} centers in the HS state and remains constant down to 198 K. Then, upon cooling, $\chi_M T$ decreases in two marked steep steps to ca. 0.12 cm^3 K mol^{-1} at 170 K indicating the occurrence of a complete HS→LS spin transition. The heating mode does not match the cooling mode showing a narrow asymmetric hysteresis loop (ca. 6 K in average). The equilibrium temperatures $T_{1/2}$, at which the molar fractions of the HS and LS species are equal to 50%, are $T_{1/2}^{\downarrow}$ = 189 K and $T_{1/2}^{\uparrow}$ = 195 K for the cooling and heating modes, respectively, measured at a temperature scan rate of 1 K min^{-1}.

The temperature dependence of the $\chi_M T$ product for compound **2** measured at 1 K min^{-1} is displayed in Figure 1-bottom. At 300 K, the $\chi_M T$ value is ca. 3.35 cm^3 K mol^{-1} and remains constant down to 220 K. Then gradually decreases, upon cooling, attaining a value of 0.84 cm^3 K mol^{-1} at 50 K. Below this temperature $\chi_M T$ decreases slightly most probably due to the zero-field splitting of the Fe^{II} centers that remain HS at low temperatures. Indeed 75% of the Fe^{II} centers undergo spin transition from the HS state to the LS state in **2**. In the heating mode $\chi_M T$ does not match the values observed for cooling mode showing an unsymmetrical hysteresis in the low temperature range (ca. 100-150 K), which practically disappears at higher temperatures. This behavior could be attributed to steric effects induced by the nitrobenzene molecules hosted in the pores and small kinetic effects that do not allow the system to reach the thermodynamic equilibrium even at temperature scan rates of 1 K min^{-1}. Considering a hypothetical complete SCO for **2**, the equilibrium temperatures are $T_{1/2}^{\downarrow}$ = 145 K and $T_{1/2}^{\uparrow}$ = 152 K.

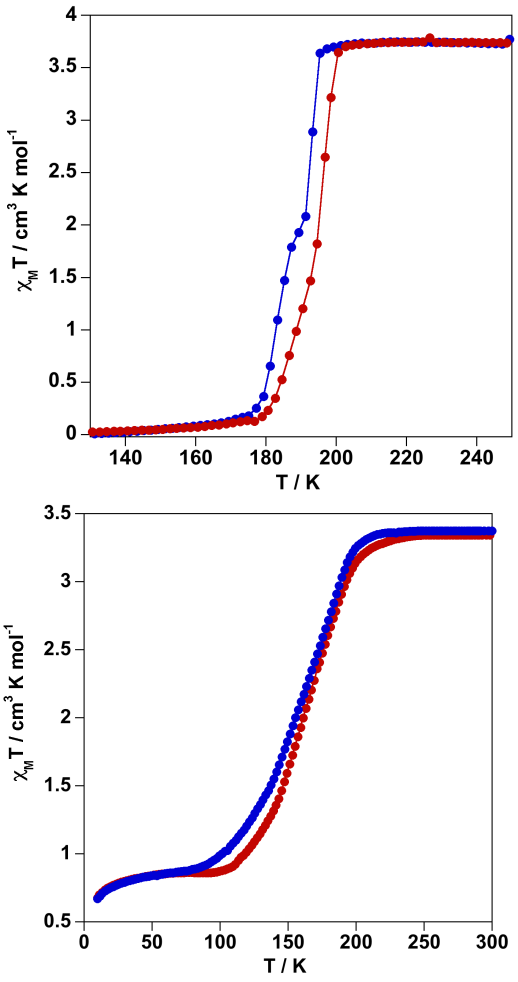

Figure 1 Magnetic behaviour displayed by **1** (top) and **2** (bottom). The cooling and heating modes are shown in blue and red colours, respectively.

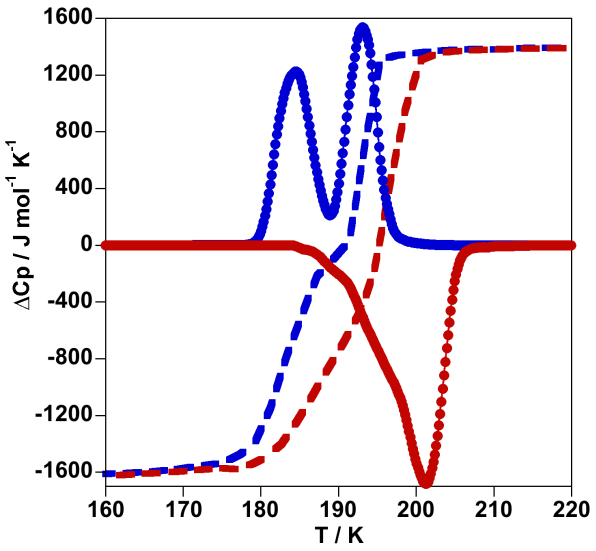

Figure 2. Calorimetric properties for compound **1**. The magnetic behavior of **1** has been included as reference (dashed lines). Blue and red lines correspond to the cooling and heating modes, respectively.

Calorimetric studies. DSC measurements were carried out for **1**. The temperature scan rate in the cooling and heating modes was 10 K min^{-1}. The anomalous variations of the molar specific heat due to SCO, in the form of ΔC_p vs T plot, for the cooling and heating modes is displayed in Figure 2. The ΔC_p vs. T plot shows the presence of two well separated peaks in the cooling mode whereas in the heating mode the peaks overlap and reflect the changes in the slope observed in the $\chi_M T$ vs. T curve of **1**. Moreover, each peak is reminiscent of those observed in the $\partial(\chi_M T)/\partial T$ vs. T plot (Figure S2, Supporting Information). The obtained critical temperatures ($T_{1/2}^{\downarrow}$ = 188 K and $T_{1/2}^{\uparrow}$ = 201 K) reproduces those obtained from the magnetic data. The average enthalpy and entropy variations associated with the cooling and heating modes, ΔH = 14.0 kJ mol^{-1} and ΔS = 71.6 J K^{-1} mol^{-1}, are consistent with the values typically displayed by Hofmann-like clathrates of Fe^{II} featuring strong cooperative SCO behavior.[6] The DSC measurements could not be performed on **2** because the temperature window of the spin transition for this compound extends beyond the limits of our calorimeter.

Structure. X-ray single-crystal studies were carried out for **1** at 150 and 250 K and for **2** at 250 K. A selection of significant bond lengths [Å] and angles [°] and relevant crystallographic data are collected in Tables 1-3, respectively.

Compound **1** displays the monoclinic non-centrosymmetric *Pc* space group irrespective of temperature. The structural motifs in this material are essentially the same at both temperatures; thus, the crystal structure at 150 K is representatively analysed and compared with that found at 250 K. All iron atoms are crystallographically equivalent whereas three independent Ag atoms can be seen in the asymmetric unit at both temperatures. Each iron atom defines an axially elongated [FeN$_6$] octahedron with its axial positions occupied by two nitrogen atoms of two equivalent *2,6-naphthy* ligands. The equatorial positions are occupied by four nitrogen atoms of two equivalent pairs of [Ag(CN)$_2$]$^-$ and [Ag$_2$(CN)$_3$]$^-$ groups (Figure 3). The average bond length <Fe-N> is, respectively, 1.96 Å and 2.18 Å at 150 and 250 K. This corresponds to a variation of ca. 0.22 Å between the LS and HS states, which is consistent with a complete spin transition. The sum of deviations from the ideal octahedron of the 12 "cis" N–Fe–N angles ($\sum = \sum_{i=1}^{12}|\theta_i - 90|$) shows that the coordination center is weakly distorted in the HS state with $\sum$ = 24.3° and this value decreases slightly in the LS state down to 22.8°.

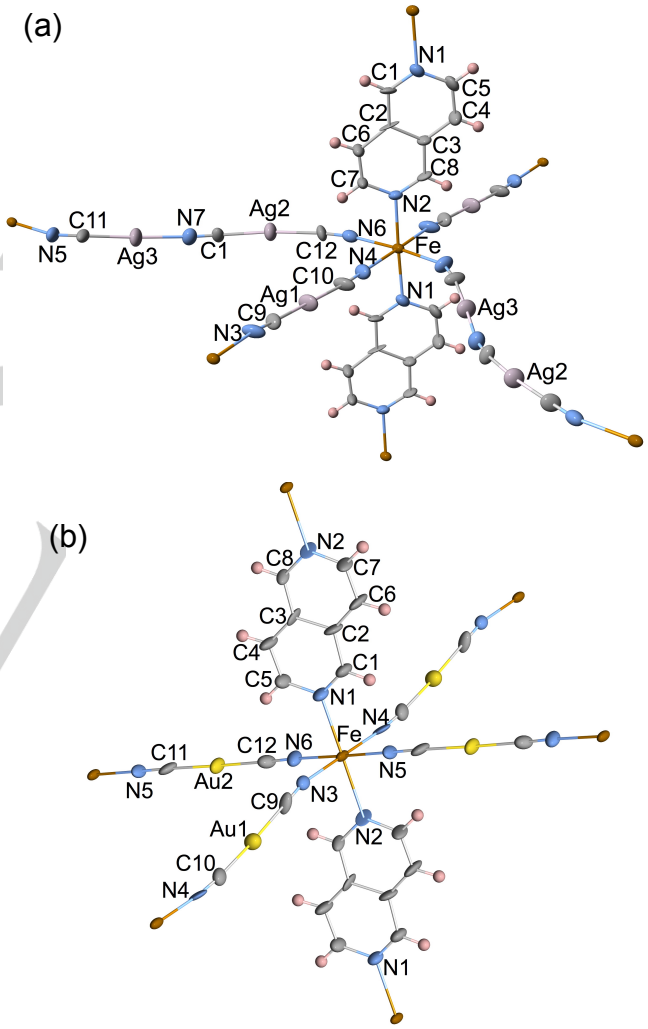

Figure 3. ORTEP representation of the representative molecular fragment for compounds **1** (a) and **2** (b) (thermal ellipsoids are given at 40% probability).

The equatorial [Ag(CN)$_2$]$^-$ and [Ag$_2$(CN)$_3$]$^-$ units act as bis-monodentate bridges connecting equivalent [FeN$_6$] thereby defining an infinite set of parallel {Fe[Ag(CN)$_2$][Ag$_2$(CN)$_3$]}$_\infty$ flat layers which stack along [100] direction. The grids are defined by {Fe[Ag^I(CN)$_2$][Ag$^I_2$(CN)$_3$]}$_4$ rectangular motifs (Figures 4a,b).

The almost linear $[Ag^{I}(CN)_2]^-$ anions connect the Fe^{II} centers along the [010] direction with Fe···Fe distances of 10.255(6) Å and 10.624(3) Å at 150 and 250 K, respectively. In contrast, the markedly bent conformation of the $[Ag_2(CN)_3]^-$ anions lead to corrugated -[Fe-$[Ag_2(CN)_3]$-Fe]- chains running along [001] with Fe···Fe distances of 15.0(2) Å (150 K) and 15.25(8) Å (250 K) (Figure 4a). In turn, the *2,6-naphthy* ligands, axially coordinated to the iron atoms (Fe···Fe distances are 8.991(7) Å and 9.376(4) Å at 150 and 250 K, respectively (Figure 4c)), pillar the alternate layers along [100] thus defining an open 3D framework with the distorted topology of α-Po. In addition, these links "thread" the meshes of two adjacent networks allowing the triple interpenetration of three identical 3D networks (Figure 4d). Moreover, coupled with the SCO phenomenon, strong argentophilic interactions take place between these 3D networks (Figure S3, Supporting information).

Table 1. Selected bond lengths [Å] for **1** and **2**.

	1 (250 K)	1 (150 K)	2 (250 K)
Fe-N(1)	2.264(14)	2.006(14)	2.242(13)
Fe-N(2)	2.228(13)	2.01(2)	2.237(13)
Fe-N(3)	2.147(14)	1.91(2)	2.134(14)
Fe-N(4)	2.148(14)	1.931(14)	2.14(2)
Fe-N(5)	2.14(2)	1.95(2)	2.127(12)
Fe-N(6)	2.16(2)	1.95(2)	2.158(14)
Ag(1)-C(9)	2.048(14)	2.04(2)	
Ag(1)-C(10)	2.06(2)	2.03(2)	
Ag(2)-C(12)	2.04(2)	2.05(2)	
Ag(2)-C(13)	2.06(2)	2.08(2)	
Ag(3)-C(11)	2.02(2)	2.03(2)	
Ag(2)-N(7)	2.08(2)	2.09(2)	
Ag(1)-Ag(2)	3.121(2)	3.024(3)	
Ag(1)-Ag(3)	3.281(2)	3.147(3)	
Ag(2)-Ag(3)	3.236(2)	3.114(2)	
Au(1)-C(9)			2.02(2)
Au(1)-C(10)			1.97(2)
Au(2)-C(11)			1.96(2)
Au(2)-C(12)			1.98(2)
Au(1)-Au(2)			3.1606(12)
$[FeN_6]^{av}$	2.181	1.960	2.173

The structural analysis of **2** performed at 250 K shows that this compound crystallizes in the triclinic *P*-1 space group and contains one equivalent Fe^{II} center. The iron atom defines an elongated $[FeN_6]$ octahedron equatorially coordinated by two pairs of crystallographically independent $[Au(CN)_2]^-$ groups whereas the axial positions are occupied by two equivalent *naphthy* ligands (Figure 5). The average <Fe-N> bond length of 2.17(2) Å is consistent with Fe^{II} centers in the HS state, in agreement with the magnetic data at the same temperature. The angular distortion represented by the parameter $\sum$ = 9.2º indicates that the octahedron is even more regular than for **1**.

The equatorial $[Au(CN)_2]^-$ groups act as bridges linking the Fe centers thereby defining a 2D $\{Fe[Au(CN)_2]_2\}_\infty$ grid-layered structure laying parallel to the *bc* plane. The grid structure is made up of edge-shared $\{Fe_4[Au(CN)_2]_4\}$ rhombuses defined by iron atoms and $[Au(CN)_2]^-$ linkers (Fe···Fe distances are 10.497(3) and 10.475(3) Å). The almost flat layers stack along [100] and are pillared by the *2,6-naphthy* ligands through the axial positions of the Fe centers which form chains propagating along the *a* axis where the Fe···Fe distance mediated by *2,6-naphthy* is 9.455(3) Å (Figure 5). The resulting 3D α-Po type framework exhibits a much more regular geometry than described for **1**.

Table 2. Selected angles [º] for **1** and **2**.

	1 (250 K)	1 (150 K)	2 (250 K)
N(1)-Fe-N(2)	178.3(5)	178.4(6)	178.3(5)
N(1)-Fe-N(3)	87.5(5)	88.1(6)	89.7(5)
N(1)-Fe-N(4)	90.8(6)	90.4(6)	90.6(5)
N(1)-Fe-N(5)	87.7(6)	89.0(6)	89.8(5)
N(1)-Fe-N(6)	91.8(5)	91.1(6)	89.3(5)
N(2)-Fe-N(3)	91.4(5)	91.2(6)	88.9(6)
N(2)-Fe-N(4)	90.3(6)	90.3(6)	90.8(5)
N(2)-Fe-N(5)	91.1(6)	89.7(6)	89.2(5)
N(2)-Fe-N(6)	89.6(5)	90.4(6)	91.7(5)
N(3)-Fe-N(4)	176.1(8)	178.1(6)	179.5(5)
N(3)-Fe-N(5)	94.5(7)	94.9(7)	90.7(5)
N(3)-Fe-N(6)	92.3(7)	93.2(7)	89.6(5)
N(4)-Fe-N(5)	88.9(7)	86.3(7)	88.9(6)
N(4)-Fe-N(6)	84.2(6)	85.6(7)	90.8(6)
N(5)-Fe-N(6)	173.1(5)	171.9(6)	179.1(5)
C(9)-Ag1-C(10)	176.4(9)	175.7(9)	
C(12)-Ag(2)-C(13)	171.6(7)	170.0(7)	
C(11)-Ag3-N(7)	177.2(8)	175.6(8)	
N(3)-C(9)-Ag(1)	178(2)	178(2)	
N(4)-C(10)-Ag(1)	174(2)	176(2)	
N(6)-C(12)-Ag(2)	175(2)	169(2)	
N(7)-C(13)-Ag(2)	173(2)	173(2)	
N(5)-C(11)-Ag(3)	171(2)	164(2)	
C(9)-Au(1)-C(10)			176.9(8)
C(11)-Au(2)-C(12)			177.9(7)
N(3)-C(9)-Au(1)			179(2)
N(4)-C(10)-Au(1)			176(2)
N(5)-C(11)-Au(2)			178(2)
N(6)-C(12)-Au(2)			178(2)
Σ	24.3	22.8	9.2

The large void space generated by the framework allows interpenetration of two identical 3D networks. The iron atoms of one $\{Fe[Au(CN)_2]_2\}_\infty$ layer are situated below/above but displaced from the center of the $\{Fe_4[Au(CN)_2]_4\}$ square grids belonging to the other layer (Figure 10a). Interestingly, strong aurophilic interactions (Au···Au distance is ca. 3.16(1) Å) are observed between two perpendicular edges of the $\{Fe_4[Au(CN)_2]_4\}$ square grids of two closest layers (Figure S4, Supporting Information). Despite the interpenetration, this 3D expanded Hofmann-like topology displays a channel along the *c* axis in which disordered nitrobenzene molecules are located (Figure 5-bottom). Short C···C contacts (smaller than the sum of the van der Walls radii of ca. 3.7 Å) evidence the occurrence of host-guest π-π intermolecular interactions (Figure S5 and Table S1, Supporting Information). After removing the guest molecules by SQUEEZE the void space is calculated as 348.6 $Å^3$ per unit cell, which corresponds to 34.3% of the total volume. The analysis of the crystal structure of **2** near the LS state was not possible due to the crack of the single crystals at low temperature.

Discussion

Fe^{II} Hofmann-like 3D SCO-CPs derived from $[M^{I}(CN)_2]^-$ (M^{I} = Ag, Au) building blocks have been subject of less attention than those constituted of $[M^{II}(CN)_4]^{2-}$ (M^{II} = Ni, Pd, Pt) building blocks. $[M^{I}(CN)_2]^-$ (M^{I} = Ag, Au) linkers generate more open frameworks

than $[M^{II}(CN)_4]^{2-}$ a fact that favors interpenetration and reduces the effective size of the pores. In addition, the $[Ag(CN)_2]^-$ linker is not coordinatively inert being able to expand the coordination number from 2 (linear) to 3 (T-shaped or trigonal)[15] and even 4 (tetrahedral),[16] thereby affording more complex 3D networks. Furthermore, in rare cases the $[Ag(CN)_2]^-$ acts as a chemically unstable anion affording in situ generated $[Ag_2(CN)_3]^-$ species. The first observation of this building block in a SCO-PC was described for the compound {Fe(*pmd*)[Ag(CN)$_2$][Ag$_2$(CN)$_3$]} (*pmd* = pyrimidine).[17] Compared to the title compound **1**, replacement of the organic linear linker *2,6-naphthy* with an angular linker such as *pmd*, with distinct orientation of the N donor atoms, originates a very different and complicated 3D framework.

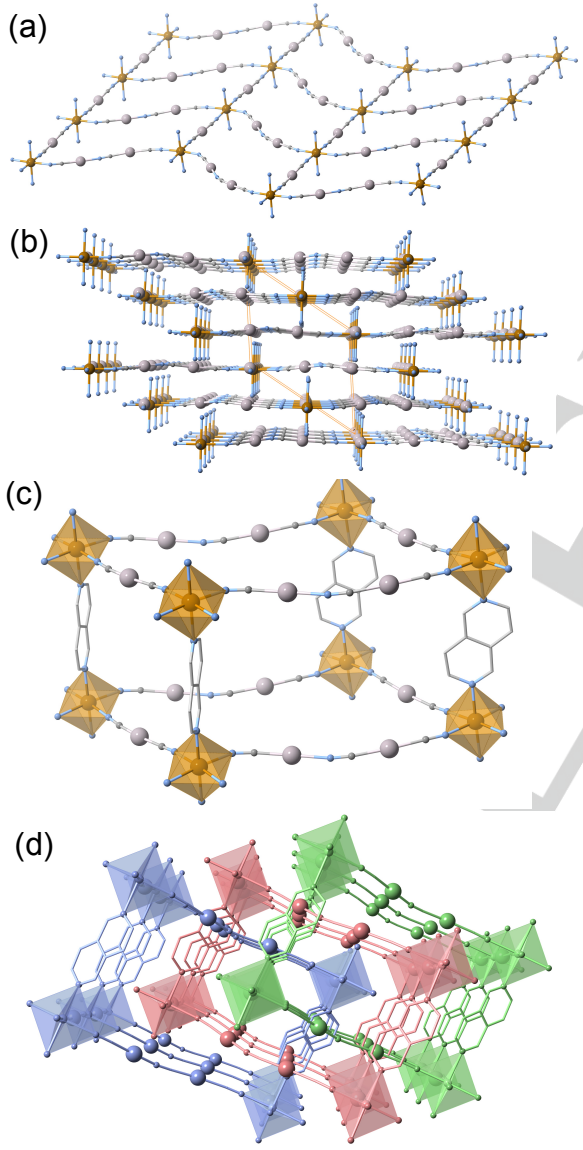

Figure 4. Compound **1**: (a) Fragment of a flat layer {Fe[Ag^I(CN)$_2$][Ag$^I_2$(CN)$_3$]}$_\infty$. (b) Two layers pillared by the 2,6-naphthy ligands. (d) Three interpenetrated α-Po type frameworks. (Yellow = Au, blue = N, grey = C, orange = Fe).

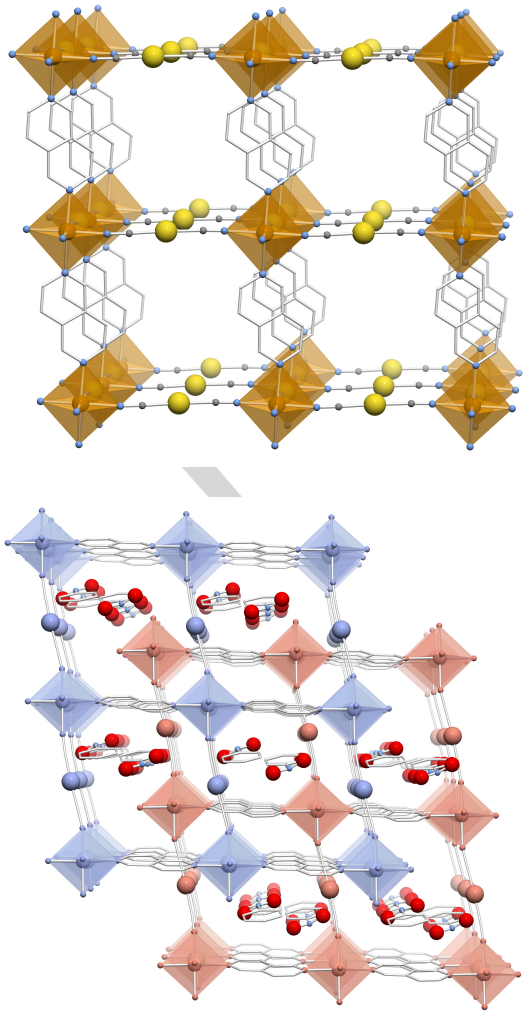

Figure 5. Compound **2**: (Top) Fragment of the 3D framework with the α-Po type network. (Bottom) Interpenetration of two identical network showing intercalated nitrobenzene molecules. (Yellow = Au, blue = N, grey = C, orange = Fe).

In both cases the organic ligand acts as a bis-monodentate bridge generating infinite -[Fe-*2,6-naphthy*-Fe]-$_\infty$ or -[Fe-*pmd*-Fe]-$_\infty$ parallel chains (Scheme 2). However, the ligand pmd imposes a 62º dihedral angle between the equatorial coordination planes of [FeN$_6$] occupied by $[Ag(CN)_2]^-$ and $[Ag_2(CN)_3]^-$ units (Scheme 2), making impossible to form a simple stack of pillared layers {Fe[Ag(CN)$_2$][Ag$_2$(CN)$_3$]} as described for **1**, and thereby generating an intricate self-interpenetrated 3D CP. It is interesting to remark that using the slightly shorter *pz* ligand instead of *2,6-naphthy* does not favor the formation of $[Ag_2(CN)_3]^-$ giving {Fe(*pz*)[Ag(CN)$_2$]$_2$}, which exhibits the prototypal double interpenetrated α-Po networks shown in Scheme 1. In contrast, $[Ag_2(CN)_3]^-$ is generated from self-assembling Cd^{II}, *pz* and $[Ag(CN)_2]^-$ affording the compound {Cd^{II}(*pz*)[Ag(CN)$_2$][Ag$_2$(CN)$_3$]},[18] which shares with the title compound **1** the triply interpenetrated expanded version of {Fe(*pz*)[Ag(CN)$_2$]$_2$}.[7]

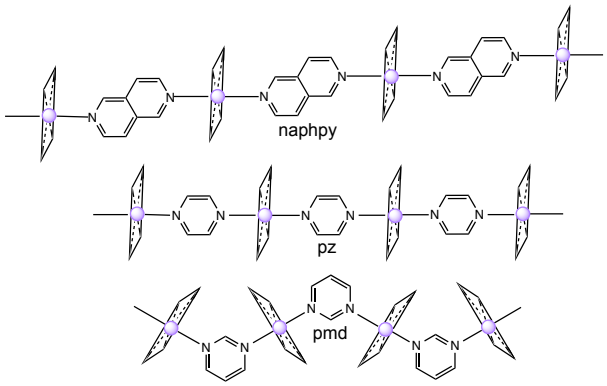

Scheme 2. Propagation of the $\{Fe(L)\}_n$ chains defined by the organic bis-monodentate bridging organic ligand L (see text).

There are two additional examples of 3D SCO-CP exhibiting the $[Ag^{I}_2(CN)_3]^-$ building block. One is the compound $\{Fe(3,5\text{-}CH_3py)_2[Ag_2(CN)_3][Ag(CN)_2]\}$ (*3,5-CH₃py* = 3,5-dimethylpyridine) in which the monodentate nature of the axial organic ligand transforms the Fe^{II} centers into planar nodes with coordination number 4 affording an expanded version of the prototypal structure of $CdSO_4$.[14b] Given the open nature of this framework, the crystal packing of the *3,5-CH₃py* derivative consists of three identical interpenetrated subnets. The other example is $\{Fe(dpb)[Ag(CN)_2][Ag_2(CN)_3]\}\cdot$nSolv where *dpb* is the long bridging ligand 1,4-di(pyridin-4-yl)benzene (Scheme 1).[14c] This compound displays a very complicated porous 3D framework that can be deconstructed into two identical interpenetrated networks with the topology of $CdSO_4$ in which the "pseudo-square" planar Fe^{II} nodes are defined by the *dpb* and $[Ag(CN)_2]^-$ bridges, while the $[Ag_2(CN)_3]^-$ groups can be seen as connectors between the two $CdSO_4$ subnets.

A common characteristic of the pmd, *3,5-CH₃py* and *2,6-naphthy* SCO-CPs is the occurrence of more or less marked incipient two-step SCO. Moreover, the title compound **1** displays a moderate cooperativity characterized by an unsymmetrical hysteresis loop ca. 6 K wide. In contrast, the *dpb* derivative with the organic bridging ligand longer favors the presence of voids occupied by solvents, which influence the completeness of the transition. In particular, for $\{Fe(dpb)[Ag(CN)_2][Ag_2(CN)_3]\}\cdot 2DMF\cdot CH_3CN$ the two-step SCO extends over a wide interval of temperatures, 200-75 K, exhibiting hysteresis loops ca. 10 K wide. Apparently, the presence of $[Ag(CN)_2]^-$ and $[Ag_2(CN)_3]^-$ anions confers some degree of flexibility to the framework allowing accommodation of the $[FeN_6]$ structural changes during the SCO, a fact that explains the lack of strong cooperative SCO and larger hysteresis in this series.

The inertness of the $[Au(CN)_2]^-$ building block against dissociation and/or increase of the coordination number makes its structural chemistry much more predictable than that described for $[Ag(CN)_2]^-$. Independently of the bridging organic ligand length, all derivatives so far reported can be generically formulated $\{Fe(L)[Au(CN)_2]_2\}\cdot$Guest with *L* = *bipytz*,[10a] *bipydz*,[10a,b] *bpp*,[12] *dpb*,[13] *pz*[8] and *Fpz*[9] (Scheme 1). In the same way as the herein reported compound **2**, all these derivatives share the same structural feature consisting of twofold interpenetrating α-Po networks already discussed for $\{Fe(pz)[Ag(CN)_2]_2\}$ (Scheme 1). For the shortest members of the series, pz and Fpz, the resulting more densely packed framework without accessible voids, show highly cooperative SCO properties exhibiting, respectively, ca. 20 and 40 K wide hysteresis loops at relatively high temperatures. However, the cooperativity decreases markedly for the remaining members of the series as the length of the organic bridging ligand increases. Nevertheless, it has been shown that the presence of suitable guest molecules in the pores modulates and enhances the cooperative response of the material in the *bpp*, *dpb* and *bipytz* derivatives. Although the size of the *2,6-naphthy* ligand is closer to the size of *pz* and *Fpz* than *bipydz*, *dpb* or *bpp* ligands, the resulting compound **2** displays the presence of characteristic 1D channels running along [001] housing 1/2 nitrobenzene molecule per Fe^{II} which displays short π-π interactions with the host *2,6-naphthy* ligand. Furthermore, interpenetration leads to aurophilic interactions between the nets in **2** ($Au^{I}\cdots Au^{I}$ distances are ca. 3.16 Å), which are significantly shorter than observed for the *pz* and *Fpz* counterparts.

Conclusions

Two novel bimetallic Fe^{II}-M^{I} (M^{I} = Ag and Au) cyano-bridged 3D frameworks based on the ditopic *2,6-Naphthy* ligand namely $\{Fe(2,6\text{-}naphthy)[Ag(CN)_2][Ag_2(CN)_3]_2\}$ (**1**) and $\{Fe(2,6\text{-}naphthy)[Au(CN)_2]_2\}\cdot(0,5)PhNO_2$ (**2**) have been synthesized by liquid-liquid slow diffusion techniques. **1** exhibits the rare in-situ generated $[Ag_2(CN)_3]^-$ species incorporated in the $\{Fe[Ag(CN)_2][Ag(CN)_3]\}_n$ layers pillared by *2,6-naphthy* ligands that "thread" the meshes of adjacent networks and lead to a triple interpenetrated 3D framework. This densely packed structure prevents guest inclusion. Moreover, short Ag···Ag contacts take place evidencing the occurrence of argentophilic interactions between the 3D interpenetrated networks. On the other hand, **2** consists of two interpenetrated 3D networks, made up of 2D $\{Fe[Au(CN)_2]_2\}_\infty$ layers pillared by *2,6-naphthy* ligands axially coordinated to the Fe^{II} ions. Interestingly, 1D channels within this pillared structure house nitrobenzene guest molecules stabilized by host-guest π-π intermolecular interactions and strong aurophilic interactions between the interpenetrated 3D networks. **1** and **2** with different structural architectures originate two distinct SCO behaviors. **1** features a more abrupt two-step spin transition taking place in an interval of temperature 23 K wide, while **2** shows a much more gradual spin transition extending over 150 K. Despite this difference both compounds exhibit unsymmetrical hysteresis ca. 6 K wide.

Experimental Section

Materials. $K[Ag(CN)_2]$, $K[Au(CN)_2]$ and $Fe(BF_4)_2\cdot 7H_2O$ were purchased from commercial sources and used as received whereas the synthesis of

the *2,6-Naphthy* ligand was performed as it is described in Section 1.8.1 in the Supporting Information.

Crystal growth. Single crystals of 1 were grown by slow liquid-liquid diffusion technique using a modified H-vessel with a third tube. The peripheral tubes (total volume ca. 10 mL) contained Fe(BF4)2·7H2O (0.077 mmol, 26 mg) and K[Ag(CN)2] (0.154 mmol, 30.6 mg) salts, respectively. The central tube (total volume ca. 10 mL) contained 2,6-naphthy ligand (0.077 mmol, 10 mg). Each individual tube was filled with H2O:MeOH (1:1). Afterwards, the tubes were sealed with parafilm. Four weeks later, red rod-like single crystals were formed in the tube which originally contained Fe(BF4)2·7H2O salt with relative high yield (ca. 50%). $C_{13}H_6Ag_3FeN_7$ (639.69): C 24.38, H 0.94, N 15.32; found C 23.90, H 0.92, N 15.10.On the other hand, yellow rod-like single crystals of 2 (yield ca. 50%) were grown in a H-vessel tube (total volume ca. 10 mL) containing Fe(BF4)2·7H2O (0.077 mmol, 26 mg) and 2,6-naphthy ligand (0.077 mmol, 10 mg) whereas the other contained K[Au(CN)2] (0.154 mmol, 44.4 mg). Each individual tube was first filled with MeOH and secondly with a $PhNO_2$:MeOH (1:10) solution. Finally, the tubes were sealed with parafilm. The presence and quantification of the guest molecules were deduced from TGA analysis and confirmed by means of single-crystal X-ray diffraction. $C_{15}H_{8.5}Au_2FeN_{6.5}O$ (745.57): C 24.14, H 1.14, N 12.20; found C 24.51, H 1.16, N 12.35.

Physical characterization. Variable temperature magnetic susceptibility measurements were carried out by using samples (15-20 mg) consisting of single crystals of the titled compounds, using a Quantum Design MPMS2 SQUID susceptometer equipped with a 5.5 T magnet, operating at 1 T and at temperatures from 300-1.8 K.

Calorimetric measurements were performed using a differential scanning calorimeter Mettler Toledo DSC 821e. Low temperatures were obtained with an aluminium block attached to the sample holder, refrigerated with a flow of liquid nitrogen and stabilized at a temperature of 110 K. The sample holder was kept in a dry box under a flow of dry nitrogen gas to avoid water condensation. The measurements were carried out using around 20 mg of single crystals of **1** sealed in aluminium pans with a mechanical crimp. Temperature and heat flow calibrations were made with standard samples of indium by using its melting transition (429.6 K, 28.45 J g^{-1}). An overall accuracy of ±0.2 K in temperature and ±2% in the heat capacity is estimated. The uncertainty increases for the determination of the anomalous enthalpy and entropy due to the subtraction of an unknown baseline.

Single-crystal X-ray data were collected on an Oxford Diffraction Supernova. In all cases MoKα radiation (λ = 0.71073 Å) was used. A data scaling and empirical or multiscan absorption correction was performed. The structures were solved by direct methods using SHELXS-2014 and refined by fullmatrix least-squares on F^2 using SHELXL-2014.[19] Non-hydrogen atoms were refined anisotropically, and hydrogen atoms were placed in calculated positions refined using idealized geometries (riding model) and assigned fixed isotropic displacement parameters. Relevant crystallographic data for **1** and **2** are gathered in Table 3. Compound **1** shows thermal disorder at 250 and 150 K as well as residual electron density (3.68−4.49 eÅ^{-3}) located very close to the Ag sites at 150 K (alerts A and B). Nitrobenzene guest molecules show thermal disorder at 250 K (alerts A and B) for **2** and residual electron density (2.48−10.94 eÅ^{-3}) located very close to the Fe and Au atoms (alerts A and B). However, the structures of the host frameworks as well as in general those of the guest molecules are reasonably well determined. More importantly, they fully convey all the chemical and structural meaning required to explain correctly the spin crossover behavior in this series of compounds and compare well with the data reported previously for other members of the Hofmann-type spin crossover clathrate family.

CCDC 1565402-1565404 contain the supplementary crystallographic data for this paper. These data can be obtained free of charge from The Cambridge Crystallographic Data Centre.

Table 3. Crystal data for compounds **1** and **2**.

Compound	**1** (250 K)	**1** (150 K)	**2** (250 K)
Empirical formula	$C_{13}H_6Ag_3FeN_7$		$C_{15}H_{8.5}Au_2FeN_{6.5}O$
Mr	639.69		745.57
Crystal system	monoclinic		triclinic
Space group	*Pc*		*P*-1
Temperature	250 K	150 K	250 K
a (Å)	9.3760(8)	8.991(5)	9.4548(9)
b (Å)	10.6240(8)	10.255(5)	10.4730(9)
c (Å)	11.2753(9)	11.110(4)	10.4975(12)
α (°)	90	90	83.369(9)
β (°)	126.714(9)	126.22(3)	85.076(9)
γ (°)	90	90	80.288(8)
V (Å^3)	900.3(2)	826.4(7)	1015.4(2)
Z	2		2
Dc (mg cm^{-3})	2.360	2.571	2.439
F(000)	600		672
μ (Mo-Kα)(mm^{-1})	4.012	4.371	15.133
Crystal size (mm)	0.06 x 0.06 x 0.10		0.08 x 0.08 x 0.18
No. of total reflections	3389	3307	5127
No. of reflections [I>2σ(I)]	3076	3064	3187
R [I>2σ(I)]	0.0684	0.0637	0.1033
R [all data]	0.0753	0.0685	0.1402
S	1.176	0.836	1.021

R1 = Σ ||Fo| - |Fc|| / Σ |Fo|; wR = [Σ [w(Fo^2 - Fc^2)^2] / Σ [w(Fo^2)^2]]$^{1/2}$.
w = 1/ [σ^2(Fo^2) + (m P)^2 + n P] where P = (Fo^2 + 2Fc^2) / 3;
m = 0.1090 (**1** (250 K)), 0.1029 (**1** (150 K)) 0.1886 (**2** (250 K))
n = 1.5595 (**1** (250 K)), 29.0173 (**1** (150 K))

Acknowledgements

This work was supported by the Spanish Ministerio de Economia y Competitividad (MINECO), FEDER (CTQ2013-46275-P and CTQ2016-78341-P), Unidad de Excelencia María de Maeztu (MDM-2015-0538), and the Generalitat Valenciana through PROMETEO/2016/147. L.P.L. and F.J.V.M. thank, respectively, the Universidad de Valencia and a MINECO for a predoctoral (FPI) grant.

Keywords: Coordination polymers • MOFs • Hofmann Clathrates • iron(II) complexes• spin crossover

[1] a) E. König, *Struct. Bonding (Berlin)* **1991**, *76*, 51; b) P. Gütlich, A. Hauser, H. Spiering, *Angew. Chem., Int. Ed. Engl*. **1994**, *33*, 2024; c) J. A. Real, A. B. Gaspar, V. Niel, M. C. Muñoz, *Coord. Chem. Rev*. **2003**, *236*, 121; d) P. Gütlich, H. A. Goodwin, Eds. Spin Crossover in Transition Metal Compounds I-III. *Top. Curr. Chem*. **2004**, Vols. *233-235*; e) J. A. Real, A. B. Gaspar, M. C. Muñoz, *Dalton Trans.* **2005**, 2062; f) A. Bousseksou, G. Molnár, L. Salmon, W. Nicolazzi, *Chem. Soc. Rev*. **2011**, *40*, 3313; g) M. A. Halcrow, Ed. Spin-crossover materials: properties and applications. John Wiley & Sons. **2013**.

[2] C. Enachescu, M. Nishino, S. Miyashita in Spin-crossover materials: properties and applications. Halcrow, M. A. Ed. Pages 455-471; John Wiley & Sons. **2013**.

[3] a) O. Kahn, *J. Chem. Phys*. **1988**, *85*, 1113; b) O. Kahn, J. P. Launay, *Chemtronics* **1988**, *3*, 140; c) O. Kahn, J. Kröber, C. Jay, *Adv. Mater* **1992**, *4*, 718; d) O. Kahn, C. J. Martinez, *Science* **1998**, *44*, 279.

[4] a) V. Meded, A. Bagrets, K. Fink, R. Chandrasekar, M. Ruben, F. Evers, A. Bernand-Mantel, J. S. Seldenthuis, A. Beukman, H. S. J. van der Zant, *Phys. Rev. B: Condens. Mater Mater. Phys*. **2011**, *83*, 245415; b) F. Prins, M. Monrabal-Capilla, E. A. Osorio, E. Coronado, H. S. J. van der Zant, *Adv. Mater*. **2011**, *23*, 1545; c) M. Cavallini, I. Bergenti, S. Milita, J. C. Kengne, D. Gentili, G. Ruani, I. Salitros, V. Meded, M. Ruben, *Langmuir* **2011**, *27*, 4076; d) T. Miyamachi, M. Gruber, V. Davesne, M. Bowen, S. Boukari, L. Joly, F. Scheurer, G. Rogez, T. K. Yamada, P. Ohresser, E. Beaurepaire, W. Wulfhekel, *Nat. Commun*. **2012**, *3*, 938; e) P. N. Martinho, C. Rajnak, M. Ruben, In Spin-Crossover Materials: Properties and Applications; Halcrow, M. A. Ed.; Wiley: **2013**, pp 376−404 and references therein; f) H. J. Shepherd, G. Molnár, W. Nicolazzi, L. Salmon, A. Bousseksou, *Eur. J. Inorg. Chem*. **2013**, *2013*, 653; g) A. Rotaru, J. Dugay, R. P. Tan, I. A. Guralskiy, L. Salmon, P. Demont, J. Carrey, G. Molnár, M. Respaud, A. Bousseksou, *Adv. Mater*. **2013**, *25*, 1745; h) I. A. Gural'skiy, C. M. Quintero, J. Sánchez-Costa, P. Demont, G. Molnár, L. Salmon, H. J. Shepherd, A. Bousseksou, *J. Mater. Chem. C* **2014**, *2*, 2949; i) A. C. Aragonés, D. Aravena, J. I. Cerdá, Z. Acís-Castillo, H. Li, J. A. Real, F. Sanz, J. Hihath, E. Ruiz, I. Díez-Pérez, *Nano Lett*. **2016**, *16*, 218.

[5] a) J. G. Haasnoot, G. Vos, W. L. Groeneveld, *Z. Naturforsch*. B **1977**, *32*, 421; b) L. G. Lavrenova, N. V. Ikorskii, V. A. Varnek; I. M. Oglezneva, S. V. Larionov, *Koord. Khim*. **1986**, *12*, 207; c) L. G. Lavrenova, N. V. Ikorskii, V. A. Varnek; I. M. Oglezneva, S. V. Larionov, *Koord. Khim*. **1990**, *16*, 654; d) W. Vreugdenhil, J. H. van Diemen, R.A.G. De Graaff, J. G. Haasnoot, J. Reedijk, A. M. van der Kraan, O. Kahn, J. Zarembowitch, *Polyhedron* **1990**, *9*, 2971.

[6] a) J. A. Real, A. B. Gaspar, V. Niel, M. C. Muñoz, *Coord. Chem. Rev*. **2003**, *236*, 121; b) Y. Garcia, V. Niel, M. C. Muñoz, J. A. Real, Spin crossover in 1D, 2D and 3D polymeric Fe(II) networks, in: P. Gütlich, H. A. Goodwin (Eds) Spin Crossover in Transition Metal Compounds I. *Top. Curr. Chem*. **2004**, *233*, 229; c) M. C. Muñoz, J. A. Real in: M. A. Halcrow (Ed) Spin-Crossover Materials: Properties and Applications, **2013** John Wiley & Sons, Ltd. Pub. Pag. 121; d) M. C. Muñoz, J. A. Real, *Coord. Chem. Rev*. **2011**, *255*, 2068; e) M. L. Tong, *Coord. Chem. Rev*. **2017**, *335*, 28.

[7] V. Niel, M. C. Muñoz, A. B. Gaspar, A. Galet, G. Levchenko, J. A. Real *Chem. Eur. J*. **2002**, *8*, 2446.

[8] I. A. Gural'skiy, B. O. Golub, S. I. Shylin, V. Ksenofontov, H. J. Shepherd, P. R. Raithby, W. Tremel, I. O. Fritsky, *Eur. J. Inorg. Chem*. **2016**, 3191.

[9] F. J. Valverde-Muñoz, M. Seredyuk, M. C. Muñoz, K. Znovjyak, I. O. Fritsky, J. A. Real, *Inorg. Chem*. **2016**, *55*, 10654.

[10] a) J. E. Clements, J. R. Price, S. M. Neville, C. J. Kepert, *Angew. Chem. Int. Ed.* **2014**, *53*, 10164; b) J. E. Clements, J. R. Price, S. M. Neville, C J. Kepert, *Angew. Chem. Int. Ed.* **2016**, *55*, 15105.

[11] J. -Y. Li, Z. -P. Ni, Z. Yan, Z. -M. Zhang, Y. -C. Chen, W. Liu, M. -L. Tong, *Cryst. Eng. Comm.* **2014**, *16*, 6444.

[12] J. -Y. Li, Y. -C. Chen, Z. -M. Zhang, W. Liu, Z. -P. Ni, M. -L. Tong, *Chem. -Eur. J*. **2015**, *21*, 1645.

[13] J. -Y. Li, C. -T. He, Y. -C. Chen, Z. -M. Zhang, W. Liu, Z. -P. Ni, M. -L. Tong, *J. Mater. Chem.* **2015**, *C3*, 7830.

[14] a) V. Niel, A. L. Thompson, A. E. Goeta, C. Enachescu, A. Hauser, A. Galet, M. C. Muñoz, J. A. Real, *Chem. -Eur. J.* **2005**, *11*, 2047; b) T. Kosone, Y. Suzuki, S. Ono, C. Kanadani, T. Saito, T. Kitazawa, *Dalton Trans.* **2010**, *39*, 1786; c) J. -Y. Li, Z. Yan, Z. -P. Ni, Z. -M. Zhang, Y. -C Chen, W. Liu, M. -L. Tong, *Inorg. Chem.* **2014**, *53*, 4039.

[15] M. C. Muñoz, A. B. Gaspar, A. Galet, J. A. Real, *Inorg. Chem*. **2007**, *46*, 8182.

[16] A. Galet, M. C. Muñoz, A. B. Gaspar, J. A. Real, *Inorg. Chem*. **2005**, *44*, 8749.

[17] V. Niel, A. L. Thompson, A. E. Goeta, C. Enachescu, A. Hauser, A. Galet, M. C. Muñoz, J. A. Real, *Chem. Eur. J*. **2005**, *11*, 2047.

[18] T. Soma, T. Iwamoto, *Angew. Chem. Int. Ed. Engl.* **1994**, *33*, 1665.

[19] a) G. M. Sheldrick, *Acta Crystallogr. Sect. A: Found. Crystallogr.* **2008**, *64*, 112; b) G. M. Sheldrick, SHELXL-2014, University of Göttingen, Germany, **2014**.

FULL PAPER

Text for Table of Contents

The synthesis, structure, magnetic and calorimetric spin crossover (SCO) properties of doubly- and triply-interlocked iron(II) frameworks based on the bismonodentate 2,6-naphthyridine ligand are described and discussed in the frame of Hofmann-like clathrate SCO compounds.

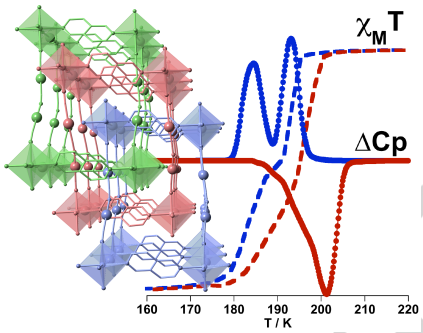

Interlocked Spin-Crossover MOFs

Lucía Piñeiro-López, Francisco-Javier Valverde Muñoz, Maksym Seredyuk, Carlos Bartual Murgui, M. Carmen Muñoz, José Antonio Real[f]*

Page No. – Page No.

Cyanide bridged Fe^{II}-M^{I} bimetallic Hofmann-like spin-crossover coordination polymers based on 2,6-Naphthyridine